Demonstration of Magnetic Dipole Resonances of Dielectric Nanospheres in the Visible Region

Andrey B. Evlyukhin,*,[†] Sergey M. Novikov,[‡] Urs Zywietz,[†] René Lynge Eriksen,[‡] Carsten Reinhardt,[†] Sergey I. Bozhevolnyi,[‡] and Boris N. Chichkov[†]

[†]Laser Zentrum Hannover e.V., Hollerithallee 8, D-30419 Hannover, Germany
[‡]Institute of Technology and Innovation, University of Southern Denmark, Niels Bohrs Allé 1E, DK-5230 Odense M, Denmark

ABSTRACT: Strong resonant light scattering by individual spherical Si nanoparticles is experimentally demonstrated, revealing pronounced resonances associated with the excitation of magnetic and electric modes in these nanoparticles. It is shown that the low-frequency resonance corresponds to the magnetic dipole excitation. Due to high permittivity, the magnetic dipole resonance is observed in the visible spectral range for Si nanoparticles with diameters of ~200 nm, thereby opening a way to the realization of isotropic optical metamaterials with strong magnetic responses in the visible region.
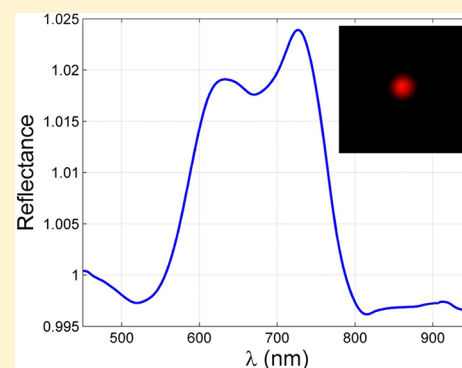
KEYWORDS: *Dielectric nanoparticles, magnetic dipole, Mie resonance, optical magnetism, metamaterials*

In modern nano-optics, nanoparticle structures are investigated for routing and manipulation of optical fields at micro- and nanoscales. Usually, metal nanoparticles are applied for these purposes due to their ability to support resonantly excited collective electron oscillations, known as localized surface plasmons (LSPs).[1,2] The strong sensitivity of LSPs to the geometry, material, and physical environment of metallic nanoparticles makes them very attractive for practical applications,[1,2] such as sensorics,[3–6] surface-enhanced Raman spectroscopy,[7] light-energy guiding along nanoparticle structures,[8] micro-optical devices for surface plasmon polaritons,[9] and nanolenses.[10–12] The excitation of individual nanoparticle LSPs in specially designed nanoparticle structures[1] opens possibilities for the creation of metamaterials with magnetic responses in the optical frequency range[13–16] and with unusual electromagnetic properties, generally not found in nature, for example, negative refraction,[16] perfect lens,[17] or object cloaking.[18]

Alternatively, the same applications can be realized with low absorbing dielectric particles having large permittivity values and supporting strong Mie resonances.[19,20] They can be considered as basic elements of complex structures and metamaterials with a desired response to electromagnetic (EM) fields, controlled by the size of particles and structural properties. Such particles can be considered as dielectric resonators (DR) or antennas, which can trap external electromagnetic fields. The incident EM energy is stored inside the dielectric particles due to resonant excitation of the corresponding DR modes. The leaky nature of the DR modes is responsible for a strong scattering at the resonant conditions. Moreover, dielectric particles can be considered as magnetic scatterers (magnetic dipoles, magnetic quadrupoles, and so on). In this case external waves resonantly excite magnetic DR modes with only magnetic radial EM field components. It is well-known from Mie theory that the first and second lowest frequency resonances of dielectric spheres correspond to the magnetic and electric dipole terms.[19,20] At these conditions dielectric spheres scatter incident EM waves into the far field as magnetic or electric dipoles. The magnetic dipole resonance occurs approximately at $\lambda/n \approx d_p$, where λ is the incident-wave vacuum wavelength, n is the particle refractive index, and d_p is the particle diameter. As it follows from the general properties of DRs,[21,22] their ability to concentrate EM energy in different modes increases with the increasing refractive index n. As a result, corresponding Q-factors for resonant modes also increase with the growing n, leading to the appearance of sharp Mie resonances in small spherical particles with a large permittivity. Thus, in contrast to metal nanoparticle structures, exhibiting usually anisotropic optical magnetic response and characterized by significant losses, dielectric particles with resonant responses have much smaller losses and can provide isotropic electromagnetically induced magnetic properties as a reaction on the magnetic component of external EM waves.[23] Magnetic characteristics of dielectric particle arrays have been theoretically considered in the work of Lewin.[24] The magnetic response of dielectric particles is especially important for the realization of negative index metamaterials with isotropic
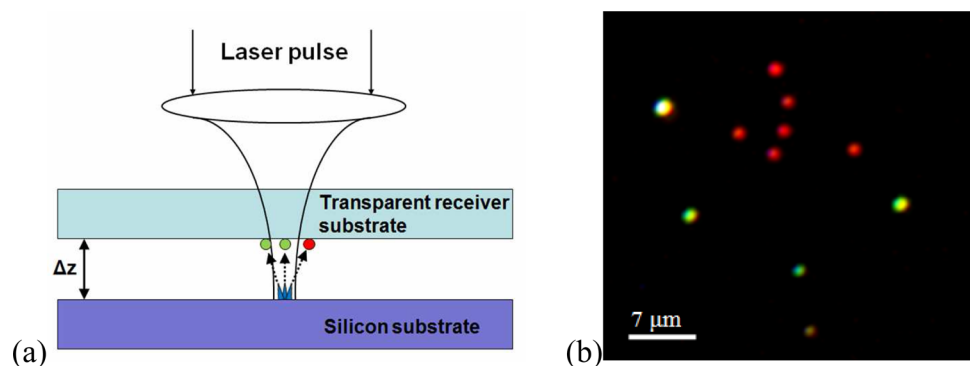
Figure 1. (a) Schematic presentation of laser induced transfer. (b) Dark-field microscope image of silicon particles fabricated by a single laser pulse on a glass receiver substrate.
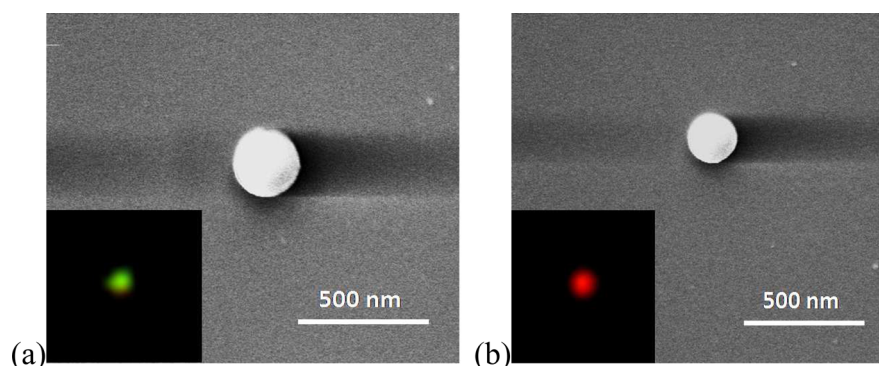

Figure 2. SEM images of spherical Si nanoparticles transferred onto a glass substrate (the images are taken at an angle of 45°). (a) $R \approx 131$ nm, (b) $R \approx 104$ nm. Insets are the corresponding dark-field images of the nanoparticles.

properties. First experimental demonstrations of dielectric metamaterials with strong magnetic properties in different spectral ranges (from microwave to mid-infrared frequencies) were recently reported.[25,26] However, an experimental demonstration of magneto-dielectric properties in the near-infrared and visible spectral ranges is still a challenging problem. So far there are only several theoretical suggestions in this field. It has been shown that a true negative index behavior can be realized at optical frequencies in metamaterials composed from silicon rods.[27] Very recently it has been shown on the basis of Mie theory that Si spherical nanoparticles, depending on their sizes, can have a strong magnetic resonance response at the visible[28] and infrared[29] frequencies. It is known[30] that for $\lambda > 450$ nm Si has dielectric properties with low absorption (the imaginary part of Si permittivity $\varepsilon''_{Si} < 1$ and quickly decreases with the increase of λ). The real part of the permittivity ε'_{Si} in the visible spectral range with $\lambda > 450$ nm takes relatively big values (ε'_{Si} is of the order of 16 to 20), so the first low-frequency Mie resonance, corresponding to the magnetic dipole (MD) mode, can be excited in Si particles with dimensions approximately 4 times smaller than the incident (vacuum) wavelength. For example, for silicon nanoparticles with a radius of ~65 nm this resonance can be excited at $\lambda \approx 550$ nm.[28] Scattering properties of Si nanostructures with Mie resonances are attracting growing interest due to their potential applications for solar cells,[31−33] for tuning optical responses of nanostructured systems,[34,35] and for field-enhanced surface spectroscopy.[36] However, so far experiments have been limited to the systems consisting of Si nanowires and nano-pillars.[31,32,35,36]

In this letter, strong optical magnetic and electric resonance responses of individual spherical Si nanoparticles with radii in the range of 100−130 nm are experimentally demonstrated, for the first time to the best of our knowledge. The Si nanoparticles are fabricated on glass substrates by laser-induced transfer (LIT)[37] and characterized using linear reflection spectroscopy with high spatial resolution.

A schematic presentation of the experimental arrangement used for LIT is shown in Figure 1a. Femtosecond laser pulses irradiate the front side of a polished silicon wafer (silicon substrate) through a transparent receiver (glass) substrate placed above the silicon wafer at a distance of $\Delta z \approx 15$ μm. Due to a localized heating of the silicon wafer, molten Si nanodroplets are formed and transferred toward the receiver substrate. These silicon nanodroplets (red and green circles in Figure 1a) are solidifying immediately on the glass surface. In our experiments, we use a commercial 1 kHz femtosecond laser system (Tsunami+Spitfire, Spectra Physics) delivering 3 mJ, 50 fs laser pulses at a central wavelength of 800 nm. After the single pulse LIT process, a random array of silicon nano-particles with sizes in the range of 200−250 nm is generated on the receiver substrate. Note that Si nanoparticles produced by the LIT method have a very thin oxide layer shell (<10 nm). A dark-field image of silicon nanoparticles on a glass substrate is shown in Figure 1b. Different colors are produced by nanoparticles with different dimensions indicating a strong dependence of scattering resonances on the particle size (Figure 2). The fabricated Si nanoparticles on the receiver substrate acquire a spherical shape due to the high surface tension of the molten silicon. Figure 2 demonstrates SEM images of two Si spherical nanoparticles with different radii.

One can see that the bigger particle has a green dark-field image (Figure 2a), whereas the smaller particle has a longer wavelength, red dark-field image (Figure 2b). At a first glance, this contradicts the expected result, since main dipole Mie resonances shift to the red side with the increasing particle size. For an Si nanoparticle with $R \approx 131$ nm, both dipole resonances are shifted to near-infrared and become invisible. As will be shown below, the green color corresponds to the resonant excitation of higher-frequency modes.

Scattering properties of the fabricated Si nanoparticles were studied using spatially resolved linear reflection spectroscopy. The experimental setup for reflection spectroscopy is described elsewhere.[38] The spectroscopic reflection analysis was performed on a BX51 microscope (Olympus) equipped with a halogen light source, polarizers, and a fiber-coupled grating spectrometer QE65000 (Ocean Optics) with a wavelength resolution of 1.6 nm. The reflected light was collected in backscattering configuration using MPlanFL (Olympus) objective with magnification ×100 (NA = 0.9). The image area analyzed by the spectrometer is limited by a pinhole with a diameter of 800 μm resulting in a circular probing area with a diameter of 8 μm. Experimental data present the R_{norm}, where R_{norm} is a ratio between spectra obtained from the place with particles and reference spectra recorded from the surface without them. The microscope images (1600 × 1200 pixels) were captured with a LC20 digital color camera (Olympus). Experimental reflection spectra were obtained with the polarized illumination and unpolarized collection. The light scattering process is schematically illustrated in Figure 3. The
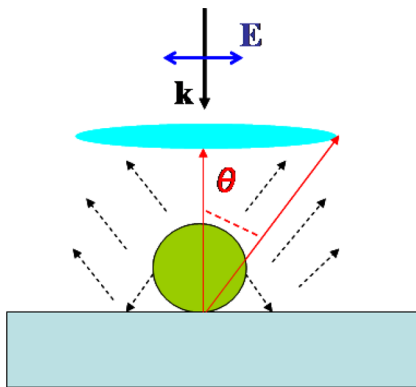

Figure 3. Schematic view of light scattering by a particle on a glass substrate irradiated by an incident light wave with a wave vector **k** and electric field **E**. The angle θ defines a conical area for the scattered light registered by the detection system.

reflected light which can be registered by the detection system is defined by the conical angle θ. Thus, for understanding the measured reflectance spectra, one should take into account angular distribution of the scattered light.

Experimental reflection spectra of Si nanoparticles, shown in Figure 2, are demonstrated in Figure 4a,b. The recorded reflection spectra are quite complex for both nanoparticles. There are two strong maxima located for the nanoparticle with $R = 132$ nm (Figure 4a) at $\lambda \approx 750$ nm and $\lambda \approx 900$ nm and for the nanoparticle with $R = 104$ nm (Figure 4b) at $\lambda \approx 625$ nm and $\lambda \approx 730$ nm, respectively. There are also several small peaks on the short wavelength side from the main maxima in Figure 4a. In spite that Si nanoparticles are located on a glass substrate and their environment is not strictly homogeneous, their

scattering spectra can be modeled by Mie theory. Due to the small area contact of spherical nanoparticles with the low refractive index glass substrate, its presence does not notably change the distribution of EM fields inside the Si nanoparticles. Moreover, recently it has been shown that, even in the case of Si nanoparticles located on a Si substrate, Mie modes can be applied for characterization of scattering spectra.[33]

In Mie theory the scattered electric field **E**, at distances larger compared to the scatterer size, can be approximated as a superposition of electric fields created by several first multipole moments of the scatterer: $\mathbf{E} \approx \mathbf{E_p} + \mathbf{E_m} + \mathbf{E_Q} + \mathbf{E_M} + ...$, where $\mathbf{E_p}$, $\mathbf{E_m}$, $\mathbf{E_Q}$, and $\mathbf{E_M}$ are the electric fields created by electric dipole **p**, magnetic dipole **m**, electric quadrupole $\hat{Q}$, and magnetic quadrupole $\hat{M}$ moments, respectively.[39] These fields in turn can be calculated using field propagators describing the electric field at a certain point created by a corresponding multipole source.[40] Thus, one can write in the far-filed approximation, taking into account only the first four multipole moments[41,42]

$$\mathbf{E}(\mathbf{r}) = \frac{k_0^2 e^{ik_0 r}}{4\pi\varepsilon_0 r}([\mathbf{n} \times [\mathbf{p} \times \mathbf{n}]] + \frac{ik_0}{6}[\mathbf{n} \times [\mathbf{n} \times \hat{Q}\mathbf{n}]]$$
$$+ \frac{1}{c}[\mathbf{m} \times \mathbf{n}] + \frac{ik_0}{2c}[\mathbf{n} \times (\hat{M}\mathbf{n})]) \qquad (1)$$

where k_0 is the wavenumber in vacuum, ε_0 is the vacuum permittivity, c is the vacuum speed of light, and $\mathbf{n} = \mathbf{r}/r$ is the unit vector directed from the scatterer to the observation point. Here we assume that the scatterer is located in air at the origin of a Cartesian coordinate system. The differential scattering cross section $\sigma_d(\mathbf{n})$ is determined as a ratio between the power scattered into the direction **n** and the incident power density. Integrating $\sigma_d(\mathbf{n})$ in the backward direction over the solid angle corresponding to the conical region in Figure 3, we can estimate the registered reflected light in the detection system. The field presentation (eq 1) allows us to analyze the role of different multipole moments in the scattering process. The electric dipole, magnetic dipole, electric quadrupole, and magnetic quadrupole moments are obtained from Mie theory[28] using corresponding polarizabilities α_p, α_m, α_Q, and α_M that are scalar values for a spherical scatterer located in a homogeneous environment. So finally we get

$$\mathbf{p} = \alpha_p \mathbf{E_{in}} \qquad \mathbf{m} = \alpha_m \mathbf{H_{in}}$$
$$\hat{Q} = \alpha_Q \frac{\nabla \mathbf{E_{in}} + (\nabla \mathbf{E_{in}})^T}{2}$$
$$\hat{M} = \alpha_M \frac{\nabla \mathbf{H_{in}} + (\nabla \mathbf{H_{in}})^T}{2} \qquad (2)$$

where $\mathbf{E_{in}}$ and $\mathbf{H_{in}}$ are the electric and magnetic fields of an incident wave at the scatterer center. Here we took into account that the tensor quadrupole moments are determined by the symmetrical parts of the electrical and magnetic field gradients $\nabla\mathbf{E_{in}}$ and $\nabla\mathbf{H_{in}}$, and T denotes the transpose operation in (eq 2). The corresponding polarizabilities can be obtained by the methods described elsewhere.[43−45]

Simulated scattering cross sections for the Si spheres in air with radii of 122 and 97 nm are presented in Figure 4c,d (the red curves with markers). The size of the particles has been chosen from the condition that the spectral positions of resonances should be close to the experimental values (Figure 4a,b). Good agreement between the theoretical simulation and
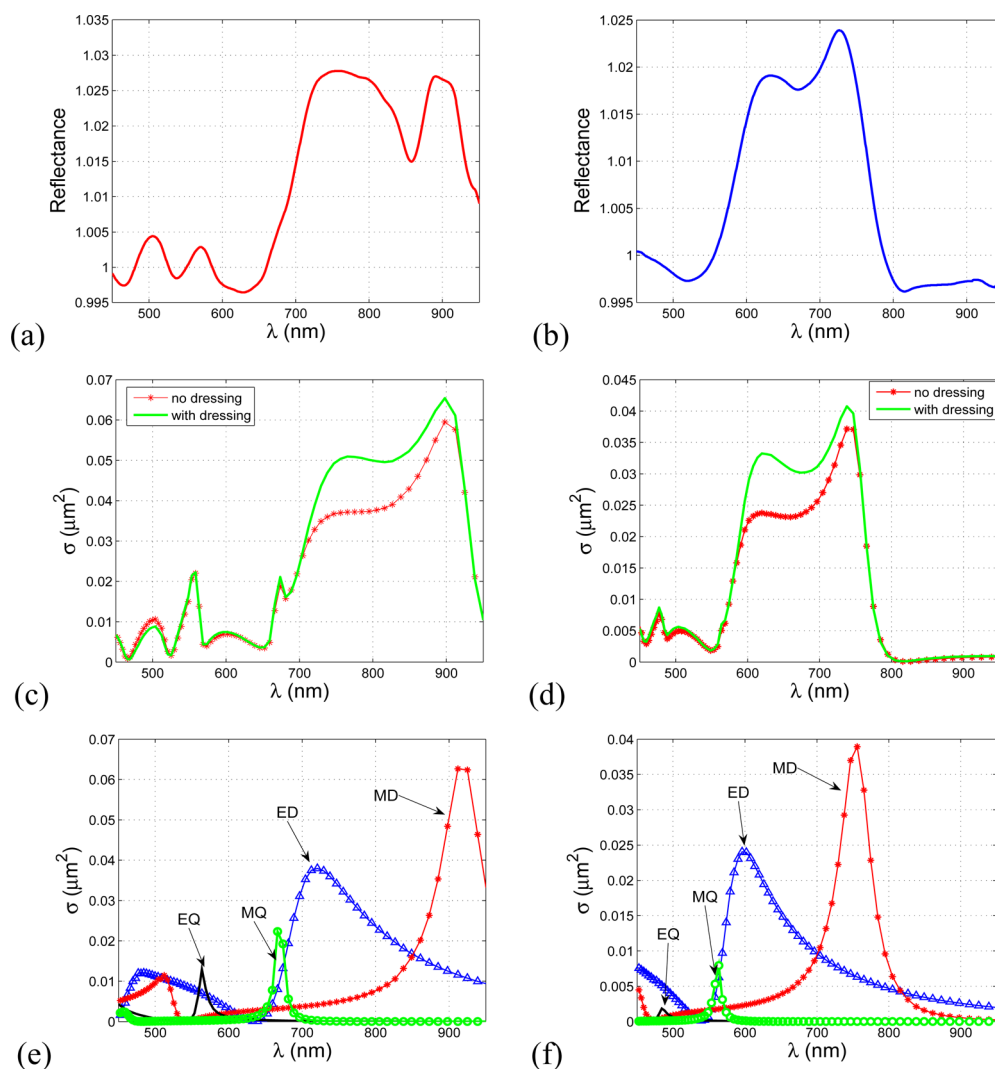
Figure 4. (a, b) Experimental reflectance spectra of Si nanoparticles with the radii of $R \approx 131$ nm (a) and $R \approx 104$ (b) nm located on a glass substrate with the refractive index $n = 1.5$. (c, d) Calculated scattering cross sections into the conical region with angle $\theta = 40°$ (Figure 3) of silicon nanoparticles presented as a point multipole scatterers (electric dipole (ED), magnetic dipole (MD), electric quadrupole (EQ), and magnetic quadrupole (MQ)) located at the nanoparticle center in air. Corresponding polarizabilities are taken from Mie theory for $R = 122$ (c) and $R = 97$ (d). (e, f) Contributions of the different multipoles to the calculated scattering cross sections for $R = 122$ (e) and for $R = 97$ (f).

experiments can be seen by comparing Figure 4 parts c and d with parts a and b. The number and positions of the main calculated resonances correspond to the experimental realization. The origins of the resonant peaks in Figures 4c,d are clarified by the decomposition of the calculated cross sections on the contribution from different multipole moments (Figure 4e,f). As it is expected, the first two low-frequency resonances correspond to the magnetic dipole end electric dipole moments. With increasing silicon nanoparticle sizes the resonances are shifted to the red. Note that the additional resonances from the blue side of main resonances correspond to the quadrupole moments. The electric quadrupole resonance (EQ) is responsible for the green color of bigger nanoparticle in Figure 2a, whereas the red color of the nanoparticle shown in Figure 2b corresponds to the main magnetic and electric dipole resonances. A weak narrow magnetic quadrupole (MQ) resonance appears on the background of a broad electric dipole resonance for both nanoparticles. Its influence on the observed scattering spectra is negligible (a small shoulder at 670 nm appears due to this resonance, see Figure 4a,c). In spite

of qualitative agreement between the experimental reflection spectra and theoretical data, there are noticeable differences between them. For example, the sizes of nanoparticles in our experiment are larger than that in simulations, and the difference between the resonant peaks of main resonances is smaller in experiment than in theory. The difference in sizes can be explained by a small oxide shell created on Si nanoparticles during the fabrication process. A thin oxide layer on a silicon surface can be formed in natural conditions.[46,47] Moreover, such an oxide layer can be created under high temperatures.[48] Figure 5 demonstrates that all resonances are shifted to the blue side if the shell thickness increases for a silicon nanoparticle with a fixed total radius. It means that the effective size of the Si nanoparticle, which determines the resonance position, decreases. The second difference can be attributed to an influence of the substrate on the electric dipole polarizability (dressing effect) and on the optical magnetic dipole response. From the method of images[49] it follows that the electric dipole polarizability of a particle near the substrate is changed due to interaction of this particle with its image with respect to the
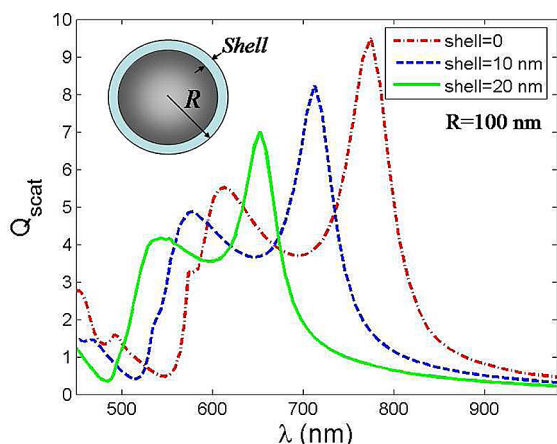
Figure 5. Scattering efficiency of silicon nanoparticles with oxide shell (refractive index 1.5) in air calculated using the Mie theory. The total radius R of the nanoparticles is fixed.

substrate surface. In particular, in the point dipole approximation[50] the dressing polarizability $\hat{a}'_p$ of dipole particle can be written as[50]

$$\hat{\alpha}'_p = \alpha_p (\hat{U} - \frac{k_0^2}{\varepsilon_0} \alpha_p \hat{G}_s(\mathbf{r}_p, \mathbf{r}_p))^{-1} \tag{3}$$

where $\hat{U}$ is the 3×3 unit tensor, $\hat{G}_s(\mathbf{r}_p, \mathbf{r}_p)$ is the part of the total Green's tensor related to the reflection from the interface and taken at the scatterer center $\mathbf{r}_p$. Using the near-field approximation[50] for $\hat{G}_s(\mathbf{r}_p, \mathbf{r}_p)$ we recalculated the scattering cross sections for Si nanoparticles using $\hat{a}'_p$ (eq 3) for the dipole polarizability. Results are presented in Figure 4c,d by the green curves without any markers. Comparing the curves in Figure 4c (Figure 4d) we see that the dressing of electric dipole polarizability of particles increases mainly the electric dipole resonant contribution in the scattering cross sections. Note that, for the electric dipole mode of Si nanoparticles, the analytical dressing polarizability can be introduced because the electric field of this mode is localized at the nanoparticle center[33] in the region smaller than the particle size. In this case the dressing effect can be estimated by eq 3 in the point dipole approximation. For the magnetic dipole mode this approach is

not applicable. For this mode, the electric field in the particle has a ring-like distribution in the plane oriented perpendicularly to the substrate surface.[33] The size of the ring is slightly smaller than the particle size. In this case, due to the interaction with substrate, the ring-distribution of the electric field can be distorted. As a result, the value of the corresponding magnetic moment can be changed, compared to the case of homogeneous environment, providing changes in the scattering spectra. Thus, differences between the main resonant peaks corresponding to the electric dipole (ED) and magnetic dipole (MD) contributions are reduced due to the substrate influence. Note that the influence of the substrate depends on its refractive index and can be evaluated in detail only by extensive numerical modeling.

The resonant optical responses of dielectric nanoparticles are accompanied by an accumulation of EM energy in excited modes. Thus, these nanoparticles can be considered as EM energy concentrators at the nanoscale dimensions, much smaller than the incident light wavelength. The energy storing capacity of nanoparticles increases with the growth of its refractive index. Figure 6a demonstrates the normalized magnetic field intensity at the center of dielectric spherical nanoparticles with the dielectric constant ε. The nanoparticles are located in air and irradiated by plane light waves. Sizes and dielectric constants of dielectric particles are chosen so that the first magnetic dipole resonance can be excited by light with $\lambda \approx 630$ nm. One can see that, at the magnetic dipole resonance, the magnetic field intensity is concentrated at the particle center (see inset in Figure 6a) and significantly increases with increasing ε. The magnetic field is more strongly localized in particles with larger ε. For example, in silicon nanoparticles with $R = 75$ nm, the magnetic field is localized in the central region of ~40 nm (Figure 6a). The distribution of electric field intensity of the magnetic dipole mode is demonstrated elsewhere.[26,33] The lifetime τ of the magnetic dipole mode in Si nanoparticles located in air can be estimated from the Lorentz distribution shown in Figure 6a, given approximately 30 fs. Note that the lifetime of dielectric particle modes decreases with increasing particle size and with increasing dielectric constant of the environment. The strong optical magnetic field is concentrated inside Si nanoparticles and can be accessible in nanoparticles with a through hole like it is shown in Figure 6b. Such holes can be produced by focused
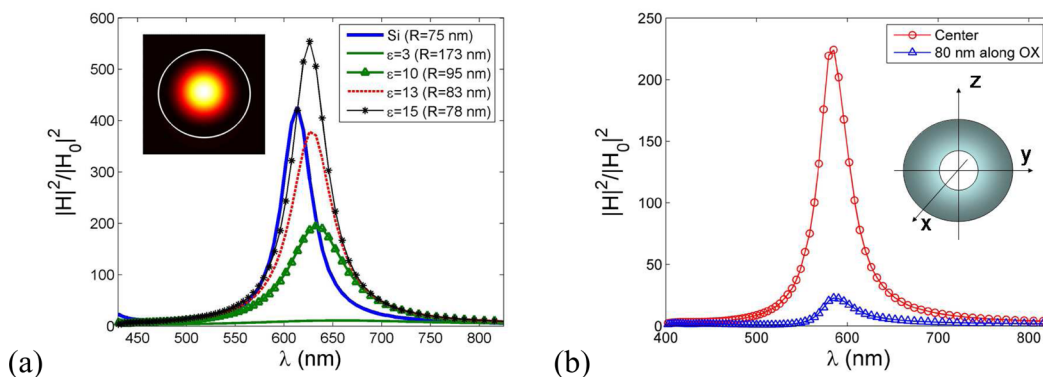

Figure 6. Calculated magnetic field intensity $|H|^2$ normalized to the incident magnetic field intensity $|H_0|^2$ in dielectric nanoparticles as a function of incident-wave wavelength: (a) at the center of dielectric spherical nanoparticles with radius R and dielectric constant ε; (b) at the center and outside of a Si spherical nanoparticle with the radius of 75 nm and a reach-through circular hole with a radius of 25 nm. The insert in part (a) demonstrates the magnetic field intensity distribution (color scale) in the cross-section of a Si nanoparticle ($R = 75$ nm) in first low-frequency (magnetic dipole) resonance ($|H|^2/|H_0|^2$).

ion-beam milling. The results shown in Figure 6b were obtained by numerical simulations using a discrete dipole approximation.[40] They demonstrate strong magnetic field enhancement at the hole center for the magnetic dipole resonance wavelength. This effect can be used for sensing and spectroscopic applications. Note that, in contrast to metal nanoparticles, where plasmon resonances are excited by the electric component of EM waves, dielectric nanoparticles are able to concentrate the optical magnetic field as a response to the magnetic component of EM waves.[23]

In summary, it has been experimentally demonstrated that spherical Si nanoparticles with diameters of ∼200 nm have the first two low-frequency Mie resonances in the visible spectral range. These resonances correspond to the excitation of magnetic and electric dipole modes. In this case the scattered EM fields produced by Si nanoparticles can be described as being generated by magnetic and electric dipolar (point-like) scatterers with polarizabilities given by the Mie theory. The optically induced magnetic properties of Si nanoparticles demonstrated in this work have important implications to the realization of isotropic optical metamaterials in the visible spectral range. In addition, individual Si nanoparticles with holes pierced through their centers can be exploited as efficient nanoantennas for the magnetic field at optical frequencies, allowing one to realize strong local magnetic-field enhancements and opening thereby new possibilities for local spectroscopies and sensing at the nanoscale.

■ AUTHOR INFORMATION

Corresponding Author
*E-mail: a.b.evlyukhin@daad-alumni.de.

Notes
The authors declare no competing financial interest.

■ REFERENCES

(1) Halas, N. J.; Lal, S.; Chang, W.-S.; Link, S.; Nordlander, P. *Chem. Rev.* **2011**, *111*, 3913−3961.

(2) Giannini, V.; Fernández-Domínguez, A. I.; Heck, S. C.; Maier, S. A. *Chem. Rev.* **2011**, *111*, 3888−3912.

(3) Haynes, C. L.; Van Duyne, R. P. *J. Phys. Chem. B* **2001**, *105*, 5599−5611.

(4) McFarland, A. D.; Van Duyne, R. P. *Nano Lett.* **2003**, *3*, 1057−1062.

(5) Lui, N.; Weiss, T.; Mesch, M.; Langguth, L.; Eigenthaler, U.; Hirscher, M.; Sönnichsen, C.; Giessen, H. *Nano Lett.* **2010**, *10*, 1103−1107.

(6) Evlyukhin, A. B.; Bozhevolnyi, S. I.; Pors, A.; Nielsen, M. G.; Radko, I. P.; Willatzen, M.; Albrektsen, O. *Nano Lett.* **2010**, *10*, 4571−4577.

(7) Zhang, W.; Cui, X.; Yeo, B.-S.; Schmid, T.; Hafner, C.; Zenobi, R. *Nano Lett.* **2007**, *7*, 1401−1405.

(8) Maier, S. A.; Atwater, H. A. *J. Appl. Phys.* **2005**, *98*, 011101.

(9) Radko, I. P.; Volkov, V. S.; Beermann, J.; Evlyukhin, A. B.; Søndergaard, T.; Boltasseva, A.; Bozhevolnyi, S. I. *Laser Photonics Rev.* **2009**, *3*, 575−590.

(10) Li, K.; Stockman, M. I.; Bergman, D. J. *Phys. Rev. Lett.* **2003**, *91*, 227402.

(11) Dai, J.; Cajko, F.; Tsukerman, I.; Stockman, M. I. *Phys. Rev. B* **2008**, *77*, 115419.

(12) Stockman, M. I. *Opt. Express* **2011**, *19*, 22029−22106.

(13) Grigorenko, A. N.; Geim, A. K.; Gleeson, H. F.; Zhang, Y.; Firsov, A. A.; Khrushchev, I. Y.; Petrovic, J. *Nature* **2005**, *438*, 335−338.

(14) Ozbay, E. *Opt. Photonics News* **2008**, *19*, 22−27.

(15) Cai, W.; Chettiar, U. K.; Yuan, H.-K; de Silva, V. C.; Kildishev, A. V.; Drachev, V. P.; Shalaev, V. M. *Opt. Express* **2007**, *15*, 3333−3341.

(16) Shalaev, V. M. *Nat. Photon.* **2007**, *1*, 41−48.

(17) Fang, N.; et al. *Science* **2005**, *308*, 534−537.

(18) Cai, W.; Chettiar, U. K.; Kildishev, A. V.; Shalaev, V. M. *Nat. Photon.* **2007**, *1*, 224−227.

(19) Van de Hulst, H. C. *Light Scattering by Small Particles*; Dover: New York, 1981.

(20) Bohren, C.; Huffman, D. *Absorption and Scattering of Light by Small Particles*; Wiley: New York, 1983.

(21) Kajfez, D.; Guillon, P. *Dielectric Resonators*; Artech House: Norwood, MA, 1986.

(22) Schuller, J. A.; Brongersma, M. L. *Opt. Express* **2009**, *17*, 24084−24095.

(23) Popa, B.-I.; Cummer, S. A. *Phys. Rev. Lett.* **2008**, *100*, 207401.

(24) Lewin, L. *Electr. Eng., Part III: Radio Commun. Eng.* **1947**, *94*, 65−68.

(25) Zhao, Q.; Zhou, J.; Zhang, F.; Lippens, D. *Mater. Today* **2009**, *12*, 60−69.

(26) Ginn, J. C.; Brener, I.; Peters, D. W.; Wendt, J. R.; Stevens, J. O.; Hines, P. F.; Basilio, L. I.; Warne, L. K.; Ihlefeld, J. F.; Clem, P. G.; Sinclair, M. B. *Phys. Rev. Lett.* **2012**, *108*, 097402.

(27) Vynck, K.; Felbacq, D.; Centeno, E.; Cbuz, A. I.; Cassagne, D.; Guizal, B. *Phys. Rev. Lett.* **2009**, *102*, 133901.

(28) Evlyukhin, A. B.; Reinhardt, C.; Seidel, A.; Luk'yanchuk, B. S.; Chichkov, B. N. *Phys. Rev. B* **2010**, *82*, 045404.

(29) Garca-Etxarri, A.; Gómez-Medina, R.; Froufe-Pêrez, L. S.; López, C.; Chantada, L.; Scheffold, F.; Aizpurua, J.; Nieto-Vesperinas, M.; Sáenz, J. J. *Opt. Express* **2011**, *19*, 4815−4826.

(30) Palik, E. *Handbook of Optical Constant of Solids*; Academic: San Diego, CA, 1985.

(31) Cao, L.; Fan, P.; Vasudev, A. P.; White, J. S.; Yu, Z.; Cai, W.; Schuller, J. A.; Fan, S.; Brongersma, M. L. *Nano Lett.* **2010**, *10*, 439−445.

(32) Garnett, E.; Yang, P. *Nano Lett.* **2010**, *10*, 1082−1087.

(33) Spinelli, P.; Verschuuren, M. A.; Polman, A. *Nat. Commun.* **2012**, *3*, 692.

(34) Cao, L.; Fan, P.; Barnard, E. S.; Brown, A. M.; Brongersma, M. L. *Nano Lett.* **2010**, *10*, 2649−2654.

(35) Seo, K.; Wober, M.; Steinvurzel, P.; Schonbrun, E.; Dan, Y.; Ellenbogen, T.; Crozier, K. B. *Nano Lett.* **2011**, *11*, 1851−1856.

(36) Wells, S. M.; Merkulov, I. A.; Kravchenko, I. I.; Lavrik, N. V.; Sepaniak, M. J. *ACS Nano* **2012**, *6*, 2948−2959.

(37) Kuznetsov, A. I.; Evlyukhin, A. B.; Reinhardt, C.; Seidel, A.; Kiyan, R.; Cheng, W.; Ovsianikov, A.; Chichkov, B. N. *J. Opt. Soc. Am. B* **2009**, *26*, B130−B138.

(38) Beermann, J.; Novikov, S. M.; Holmgaard, T.; Eriksen, R. L.; Albrektsen, O.; Pedersen, K.; Bozhevolnyi, S. I. *Opt. Express* **2012**, *20*, 654−662.

(39) Burrows, C. P.; Barnes, W. L. *Opt. Express* **2010**, *18*, 3187−3198.

(40) Evlyukhin, A. B.; Reinhardt, C.; Chichkov, B. N. *Phys. Rev. B* **2011**, *84*, 235429.

(41) Raab, R. E.; de Lange, O. L. *Multipole Theory in Electromagnetism*; Clarendon: Oxford, 2005.

(42) Chen, J.; Ng, J.; Lin, Z.; Chan, C. T. *Nat. Photon.* **2011**, *5*, 531−534 and supplementary informantion..

(43) Doyle, W. T. *Phys. Rev. B* **1989**, *39*, 9852−9858.

(44) Jylhä, L.; Kolmakov, I.; Maslovski, S.; Tretyakov, S. *J. Appl. Phys.* **2006**, *99*, 043102.

(45) Evlyukhin, A. B.; Reinhardt, C.; Zywietz, U.; Chichkov, B. N. *Phys. Rev. B* **2012**, *85*, 245411.

(46) Morita, M.; Ohmi, T.; Hasegawa, E.; Kawakami, M.; Ohwada, M. *J. Appl. Phys.* **1990**, *68*, 1272−1281.

(47) Nakamine, Y.; Kodera, T.; Uchida, K.; Oda, S. *Jpn. J. Appl. Phys.* **2011**, *50*, 115002.

(48) Deal, B. E.; Grove, A. S. *J. Appl. Phys.* **1965**, *36*, 3770−3778.

(49) Li, Z.; Gu, B.; Yang, G. *Phys. Rev. B* **1997**, *55*, 10883−10894.

(50) Evlyukhin, A. B.; Bozhevolnyi, S. I. *Phys. Rev. B* **2005**, *71*, 134304.